Electrochemistry
The Electrochemical Society of Japan
Received: August 1, 2023
Accepted: August 31, 2023
Published online: September 2, 2023
Issued: September 22, 2023
https://doi.org/10.5796/electrochemistry.23-00071
Article
Electrochemistry, **91(9)**, 097002 (2023)

Effect of Surface Structure of Graphite on the Passivation Ability of Solid Electrolyte Interphases

Yoshiho MASUDA,[a,b,*,§] Akane INOO,[b,§] Yasuyuki KONDO,[b,§] Yuko YOKOYAMA,[b,§] Yuto MIYAHARA,[b,§] Kohei MIYAZAKI,[b,§] and Takeshi ABE[b,§§]

[a] *Fuji Research Laboratory, Tokai Carbon Co., Ltd., 394-1 Subashiri, Oyama-cho, Sunto-gun, Shizuoka 410-1431, Japan*
[b] *Graduate School of Engineering, Kyoto University, Nishikyo-ku, Kyoto 615-8510, Japan*

* *Corresponding author: ymasuda@tokaicarbon.co.jp*

ABSTRACT

Solid electrolyte interphase (SEI) layer that forms on the graphite negative electrodes of lithium-ion batteries (LIBs) has a crucial role in inhibiting the excess decomposition of electrolyte solutions. While this passivating ability is essential for improving the durability of LIBs, the relationship between the passivating ability and the surface structure of the graphite is not yet fully understood. In this study, we investigate the solvent co-intercalation behavior in the presence of SEI layers formed on various types of graphite surface structures. The amount of edge sites on each graphite sample is determined using electric double layer capacitance. The co-intercalation reactions of untreated, ethylene-carbonate-treated, and vinylene-carbonate-treated graphite samples in dimethoxyethane-based electrolyte solutions are compared. The co-intercalation reactions commence at approximately 1 V vs. Li/Li^+ for all untreated samples, but the onset potentials are lowered by the presence of SEI layers, and the extent of this lowering depends on the sample. The SEI layer formed on the edge-rich surface effectively suppresses the co-intercalation reaction, and the additive is also more effective for the edge-rich sample.

Keywords : Lithium-ion Battery, Solid Electrolyte Interphase, Graphite Anode, Solvent Co-intercalation

1. Introduction

Recently, lithium-ion batteries (LIBs) have been utilized as power sources not only for portable devices, but also for electric vehicles. While there are numerous properties necessary for lithium-ion batteries in electric vehicles, long-term durability is particularly important. Solid electrolyte interphase (SEI) is formed on graphite negative electrodes through the decomposition of electrolyte solutions during the initial charging process. Once formed, the SEI suppresses solvent co-intercalation into the graphite and the excess decomposition of the electrolyte solutions.[1–3] This passivating ability is crucial to the durability of LIBs. It is well-known that the compositions of the SEI and their properties are influenced by various factors such as the electrolyte solution, electrolyte additives, and the surface structure of the graphite.[4–9] However, it remains unclear which surface structure of graphite is most suitable for forming an SEI layer with good passivating ability.

Graphite has two distinct surfaces: the edge plane and the basal plane, with lithium-ion intercalation occurring at the edge sites of the graphite.[10] In some reports, the amount of edge sites on the graphite electrode has been estimated from the electric double layer capacitance (C_{dl}), as the C_{dl} value of the edge plane is significantly larger than that of the basal plane.[11–13] The composition of the SEI layer formed on each plane has been investigated using X-ray photoelectron spectroscopy and time-of-flight secondary ion mass spectrometry, revealing that the SEI formed on the basal plane is rich in organic materials, while that formed on the edge plane is primarily composed of salt-reduction products.[14] An atomic force microscopy (AFM) study also observed that the thickness of the SEI layer formed on the basal plane of highly ordered pyrolytic graphite was thinner than that on the edge plane during the first cyclic voltammetry (CV) cycle, but in the second cycle, the SEI thickness on the basal plane became larger than that on the edge plane.[15] This result suggests that the passivating ability of the SEI layer formed on the edge plane is higher than that on the basal plane. However, it is still unclear how much passivating ability the SEI layer formed on each plane actually possesses.

In dimethoxyethane (DME)-based electrolyte solutions, lithium ions are able to insert into the graphite without forming an SEI layer on the surface of the graphite, unlike in the case of ethylene carbonate (EC)-based electrolyte solutions, which are commonly utilized in LIBs.[16,17] This process is referred to as solvent co-intercalation reaction. Previous research from our group has demonstrated that the presence of an SEI layer, formed from vinylene carbonate (VC), reduces the starting potential of the DME co-intercalation reaction and enhances the passivation ability of the SEI.[18,19] Based on this finding, the passivation ability of the SEI can be evaluated on a relative basis by measuring the starting potential of the DME co-intercalation reaction. In this study, we examine the properties of SEI layers formed on several graphite samples with distinct surface structures and measure their double layer capacitances to estimate the number of edge sites present on each sample.

2. Experimental

Four types of graphite powder samples were compared: flake-like natural graphite with three different particle sizes (NG-3, NG-15, and NG-30, where the numbers denote the particle size) and artificial graphite synthesized from cokes (AG). The surface area of each

§ECSJ Active Member
§§ECSJ Fellow
A. Inoo orcid.org/0000-0002-9990-1807
Y. Kondo orcid.org/0000-0003-1103-3329
Y. Yokoyama orcid.org/0000-0002-3943-0978
Y. Miyahara orcid.org/0000-0003-4662-0996
K. Miyazaki orcid.org/0000-0001-5177-3570
T. Abe orcid.org/0000-0002-1515-8340

sample was determined using the BET method. Composite electrodes were prepared by coating copper foils of various thicknesses (20–70 µm) with slurries of the graphite material and polyvinylidene difluoride (PVdF; KF L#9130, Kureha) in a weight ratio of 9 : 1. The electrodes were dried under vacuum at 80 °C overnight and punched into disks with a 15.95 mm diameter. The electric double layer capacitance (C_{dl}) of each sample was evaluated using coin-type symmetric cells with a 1 mol dm^{-3} $(C_2H_5)_4NBF_4$ (TEABF$_4$)/propylene carbonate (PC) (Kishida Chemical, Japan) electrolyte solution. Symmetric cells were assembled using various weights of electrodes, with a weight difference of no more than 0.05 mg. The cells were cycled between 0 and 0.4 V at a constant current of 30 µA, and the double-layer capacitance per single electrode was calculated from the amount of electric charge and the voltage.

The passivation ability of the SEI layer was evaluated from the overpotential of the DME co-intercalation reaction. To form an SEI on the graphite surface, the electrodes were electrochemically treated in a 1 mol dm^{-3} $LiClO_4$/EC + DEC (1 : 1, v/v%, Tomiyama Pure Chemical Industries) electrolyte solution with or without 3 wt% VC. This pre-treatment process was carried out using cyclic voltammetry in a three-electrode cell, with the graphite composite electrodes as the working electrodes and lithium metal as the counter and reference electrodes. The potential was referenced to the lithium metal reference electrodes. The working electrode area was limited by an O-ring, with 0.74 cm^2 of it in contact with the electrolyte solution. The scan rate, scan range, and number of cycles were 0.1 mV s^{-1}, 0–3 V, and 3 cycles, respectively. After the SEI formation, the electrodes were washed with a DME (Kishida Chemical) solution and the electrolyte solution was replaced with a 1 mol dm^{-3} $LiCF_3SO_3$ (Kishida Chemical)/DME solution. In order to check the intercalating phenomena as well as the properties of SEI, cyclic voltammetry was then conducted in the potential range of 0.0–3.0 V at a scan rate of 0.1 mV s^{-1}.

3. Results and Discussions

3.1 Electric double layer capacitance

Figure 1 presents SEM images of the graphite samples. Based on these images, the particle sizes of NG-3, NG-15, NG-30, and AG appear to be approximately 3, 15, 30, and 13 µm, respectively. Figure 2 displays a typical galvanostatic charge-discharge curve of the symmetric cell. The electric double layer capacitance per single electrode (C_{dl}) was calculated using the equation $C_{dl} = 2I_d\Delta t/\Delta V$, where I_d is the discharge current, Δt is the discharge time, and ΔV is the voltage change. Figure 3 illustrates the correlation between the weights of active materials per single electrode and the capacitance. Clear linear relationships were observed, and the specific capacitance per unit weight (C_W) was obtained from the slopes. The specific capacitance per unit surface area (C_A) was also calculated using C_W and the BET surface area (SA). The values of these parameters for each sample are listed in Table 1. In the case of the natural graphite samples, the values of C_W, as well as BET-SA,

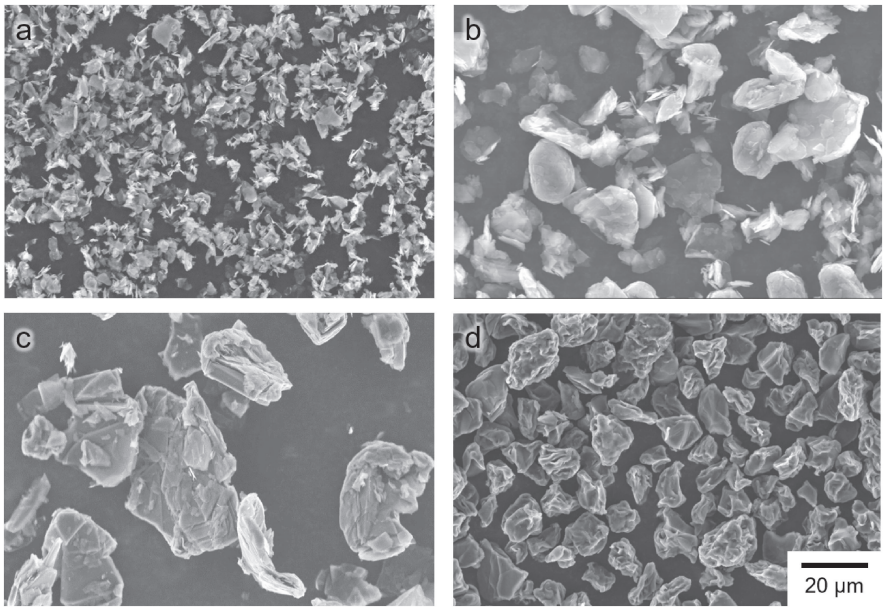

Figure 1. SEM images of (a) NG-3, (b) NG-15, (c) NG-30, and (d) AG.

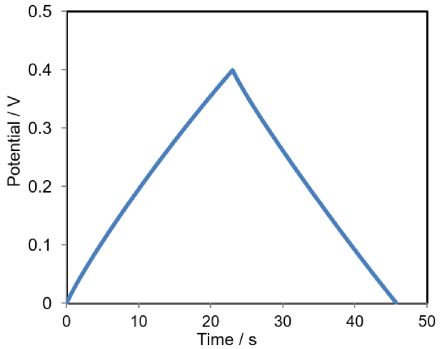

Figure 2. A typical galvanostatic charge-discharge curve for a symmetric coin cell with 1 mol dm^{-3} TEABF$_4$/PC.

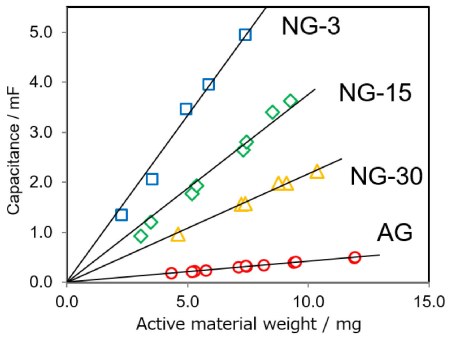

Figure 3. Correlations between weights of each active material and its capacitances.

Table 1. Parameters of the BET surface area (SA), the capacitance per unit weight (C_W) and the capacitance per unit surface area (C_A) of each sample.

Graphite samples	BET SA /$m^2\,g^{-1}$	C_W /$F\,g^{-1}$	C_A /$\mu F\,cm^{-2}$
NG-3	15	0.67	4.4
NG-15	7.2	0.38	5.2
NG-30	3.7	0.22	5.9
AG	1.4	0.04	3.0

decreased as the particle size increased, which suggests that the edge amount per unit weight also decreased as the particle size increased. Furthermore, both the C_W and C_A values of AG were notably smaller than those of the other samples, indicating that AG has a surface with a lower number of edge sites.

3.2 Electrochemical behaviors in the DME-based electrolyte solution

Figure 4 shows cyclic voltammograms for untreated graphite electrodes (black), graphite electrodes with an SEI derived from EC (blue), and those with an SEI derived from VC (red) in a 1 mol dm^{-3} $LiCF_3SO_3$/DME solution. For the untreated electrodes, the co-intercalation reactions began around 1.15 V in all samples. For all the pre-treated electrodes, the potentials at which the co-intercalation reactions began were lowered due to the presence of an SEI, as previously reported.[18,19] However, the values of these potentials varied depending on the sample. Except in the case of AG, in addition to the co-intercalation reactions, redox currents were also observed near 0 V for EC- or VC-treated electrodes, which were attributed to intercalation/deintercalation of desolvated lithium-ions. These differences among samples are originated from their surface structure.

Figure 5a illustrates the correlation between C_W and the value of the overpotential, defined as the difference between the starting potential in the absence of an SEI and in the presence of an SEI. The overpotential value increased as C_W increased, indicating that the SEI layer formed on an edge-rich surface has a good passivation ability. For VC-treated electrodes, this difference was more pronounced, with a significant increase in the overpotential value for NG-3 electrodes and only a small change observed for AG electrodes upon the addition of VC. This suggests that VC is more effective at producing a dense SEI on an edge-rich surface. These results are consistent with previous AFM studies.[15]

These differences in passivation abilities are thought to be due to the density of the SEI layers. Previously, we reported that an SEI layer formed on graphite tends to suppresses the co-intercalation of lithium ions solvated in solvents with large size such as butyl methyl triglyme, which imply that the steric hindrance of solvated ions and the density of SEI layers are the factors how easy solvated ions pass though the SEI layer.[19] On an edge-rich surface, not only is the intercalation reaction more likely to occur, but other side reactions such as the decomposition of solvents or salts are also more likely to take place.[20] Therefore, an SEI layer formed on the edge plane is thought to tend to be denser than an SEI formed on the basal plane and has a different composition, including more inorganic salts.[14] In addition, the strength of the bond between graphite and the SEI layer may also affect the passivation ability. Some functional groups which tend to be present at the edge sites affect the formation of the SEI layer especially in its early stage,[21] which may prevent an SEI layer from peeling off from graphite. As a result, solvent ions are thought to be less likely to pass through the SEI layer formed on the edge-rich surface, resulting in a larger overpotential of the co-

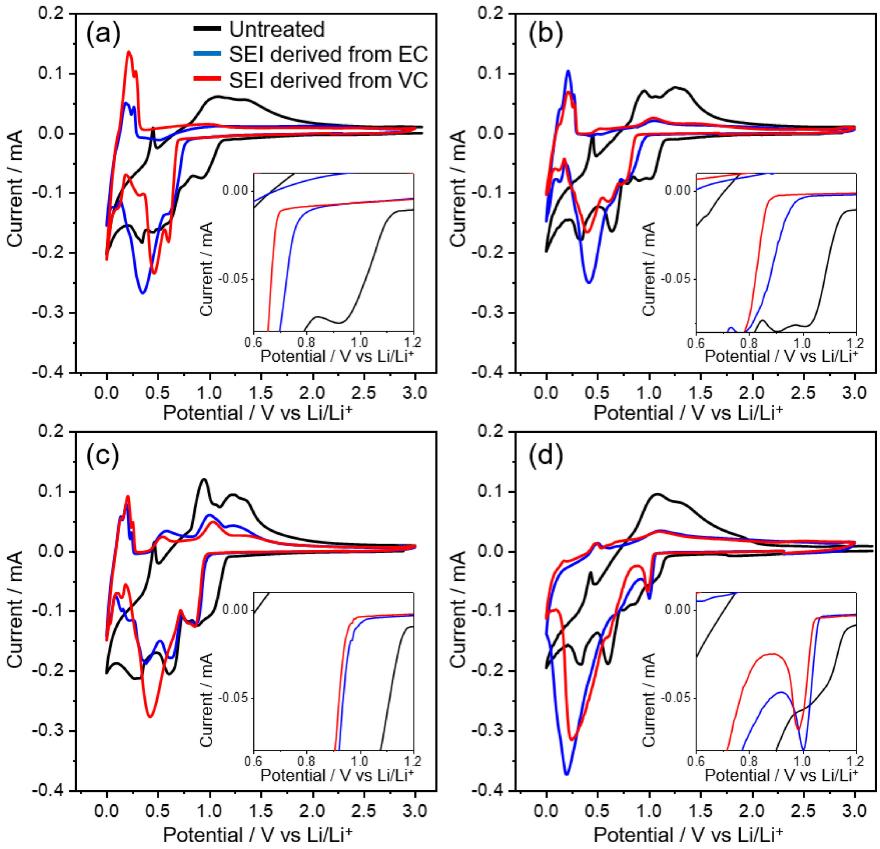

Figure 4. Cyclic voltammograms of (a) NG-3, (b) NG-15, (c) NG-30, and (d) AG in 1.0 mol dm^{-3} $LiCF_3SO_3$/DME. The black, blue and red lines indicate untreated, EC-treated and VC-treated, respectively. The insets show the enlarged views around the potential where the co-intercalation reaction began.

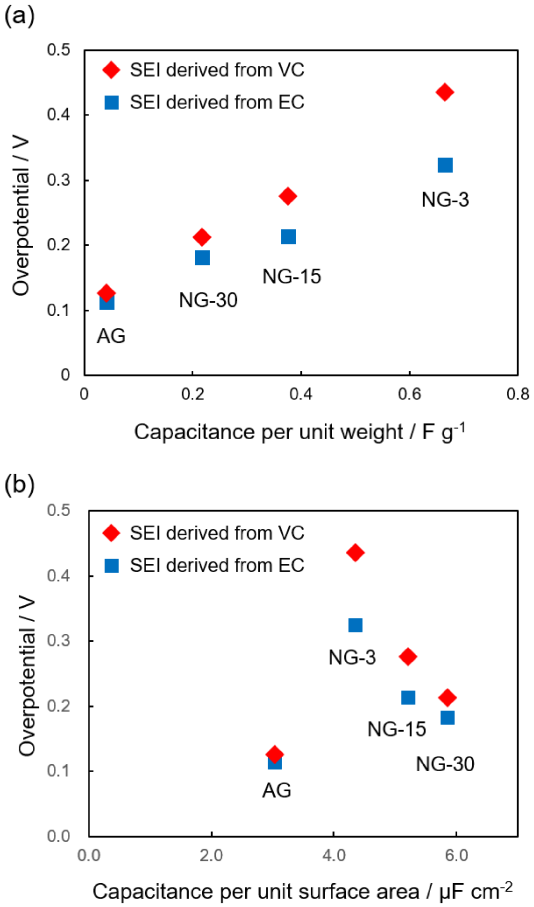

Figure 5. (a) Correlations between capacitances per unit weight and overpotentials. (b) Correlations between capacitances per unit area and overpotentials.

intercalation reaction compared to the SEI layer on basal-rich planes.

Although clear correlations were observed between C_W and the value of the overpotential, there was no clear correlation between C_A and the value of the overpotential (Fig. 5b). This might be due to the differences of the distribution of edge sites. Generally, flake-like natural graphite samples are made by milling natural graphite and strong milling is required to achieve small particle size. Then, NG-30 has a more undamaged basal plane left than NG-3 and 15, where a porous SEI layer tends to form. Since the co-intercalation reaction is considered to occur from the weak part of the SEI, the values of the overpotential of NG-30 were smaller than the values of the other natural graphite samples.

In the case of AG, redox currents due to intercalation/deintercalation of desolvated lithium-ions were barely observed. As inferred from the value of C_W and C_A, AG has an edge-poor surface, which may contribute to the ease with which the SEI layer is destroyed and peeled off from the surface during the co-intercalation reaction, rendering it ineffective as a lithium-ion conductive passivation layer. The bonding strength between the SEI layer and the graphite may also affect the passivation ability.

While the SEI layer with good passivation ability tends to form on an edge-rich surface, it cannot be assumed that an edge-rich sample is always suitable for use as a negative electrode material. Edge-rich graphite may also have a large surface area, which can lead to a high first irreversible capacity loss.[2] In the future, it may be possible to apply an amorphous carbon coating to the graphite, which has been widely used to reduce surface area, in order to balance the passivation ability of the SEI layer and the reduction of irreversible capacity loss. Amorphous carbon typically has a large number of edge sites.[22]

4. Conclusion

The passivation ability of the SEI layer on graphite samples with various surface structures was evaluated by measuring the overpotential of the DME co-intercalation reaction. The SEI layer on the edge-rich surface was more effective at suppressing co-intercalation than the one on the edge-poor surface. Additionally, the SEI-forming additive VC was more effective on edge-rich samples. These differences are thought to be due to the heterogeneity in the density of the SEI, which is caused by the distribution of edge sites. Modifying the surface of the graphite, such as through the use of an amorphous carbon coating, may be a viable method for balancing the passivation ability of the SEI layer with the reduction of irreversible capacity loss.

CRediT Authorship Contribution Statement

Yoshiho Masuda: Conceptualization (Equal), Writing – original draft (Lead)
Akane Inoo: Supervision (Supporting), Validation (Equal)
Yasuyuki Kondo: Supervision (Supporting), Validation (Equal)
Yuko Yokoyama: Supervision (Supporting), Validation (Supporting)
Yuto Miyahara: Supervision (Supporting), Validation (Supporting)
Kohei Miyazaki: Supervision (Equal), Validation (Equal)
Takeshi Abe: Supervision (Equal), Validation (Supporting)

Conflict of Interest

The authors declare no conflict of interest in the manuscript.

References

1. E. Peled, *J. Electrochem. Soc.*, **126**, 2047 (1979).
2. R. Fong, U. von Sacken, and J. R. Dahn, *J. Electrochem. Soc.*, **137**, 2009 (1990).
3. M. Tang, K. Miyazaki, T. Abe, and J. Newman, *J. Electrochem. Soc.*, **159**, A634 (2012).
4. Y. Domi, T. Doi, T. Yamanaka, T. Abe, and Z. Ogumi, *J. Electrochem. Soc.*, **160**, A678 (2013).
5. Y. Domi, M. Ochida, S. Tsubouchi, H. Nakagawa, T. Yamanaka, T. Doi, T. Abe, and Z. Ogumi, *J. Electrochem. Soc.*, **159**, A1292 (2012).
6. E. Peled, D. Golodnitsky, C. Menachem, and D. Bar-Tow, *J. Electrochem. Soc.*, **145**, 3482 (1998).
7. E. Peled, D. Bartow, A. Merson, A. Gladkich, L. Burstein, and D. Golodnitsky, *J. Power Sources*, **97–98**, 52 (2001).
8. M. Nie, D. Chalasani, D. P. Abraham, Y. Chen, A. Bose, and B. L. Lucht, *J. Phys. Chem. C*, **117**, 1257 (2013).
9. V. R. Rikka, S. R. Sahu, A. Chatterjee, P. V. Satyam, R. Prakash, M. S. R. Rao, R. Gopalan, and G. Sundararajan, *J. Phys. Chem. C*, **122**, 28717 (2018).
10. A. Funabiki, M. Inaba, and Z. Ogumi, *J. Power Sources*, **68**, 227 (1997).
11. M. T. McDermott, K. Kneten, and R. L. McCreery, *J. Phys. Chem.*, **96**, 3124 (1992).
12. A. Inoo, T. Fukutsuka, Y. Miyahara, K. Miyazaki, and T. Abe, *Electrochemistry*, **88**, 69 (2020).
13. A. Inoo, T. Fukutsuka, Y. Miyahara, Y. Kondo, Y. Yokoyama, K. Miyazaki, and T. Abe, *Electrochemistry*, **88**, 365 (2020).
14. E. Peled, D. Golodnitsky, A. Ulus, and V. Yufit, *Electrochim. Acta*, **50**, 391 (2004).
15. Y. Domi, M. Ochida, S. Tsubouchi, H. Nakagawa, T. Yamanaka, T. Doi, T. Abe, and Z. Ogumi, *J. Phys. Chem. C*, **115**, 25484 (2011).
16. T. Abe, H. Fukuda, Y. Iriyama, and Z. Ogumi, *J. Electrochem. Soc.*, **151**, A1120 (2004).
17. B. Jache, J. O. Binder, T. Abe, and P. Adelhelm, *Phys. Chem. Chem. Phys.*, **18**, 14299 (2016).
18. S. Maruyama, T. Fukutsuka, K. Miyazaki, and T. Abe, *J. Appl. Electrochem.*, **49**, 639 (2019).
19. A. Inoo, T. Fukutsuka, Y. Miyahara, Y. Kondo, Y. Yokoyama, K. Miyazaki, and T. Abe, *Chem. Lett.*, **51**, 618 (2022).
20. Y. Yamada, K. Miyazaki, and T. Abe, *Langmuir*, **26**, 14990 (2010).
21. S. H. Ng, C. Vix-Guterl, Ph. Bernardo, N. Tran, J. Ufheil, H. Buqa, J. Dentzer, R. Gadiou, M. E. Spahr, D. Goers, and P. Novák, *Carbon*, **47**, 705 (2009).
22. T. Doi, K. Miyatake, Y. Iriyama, T. Abe, Z. Ogumi, and T. Nishizawa, *Carbon*, **42**, 3183 (2004).